Tema 8. NEOTECTÓNICA

8.1. Interés de la Neotectónica en la evaluación del riesgo sísmico

8.1.1. Distribución de la actividad sísmica en la corteza terrestre

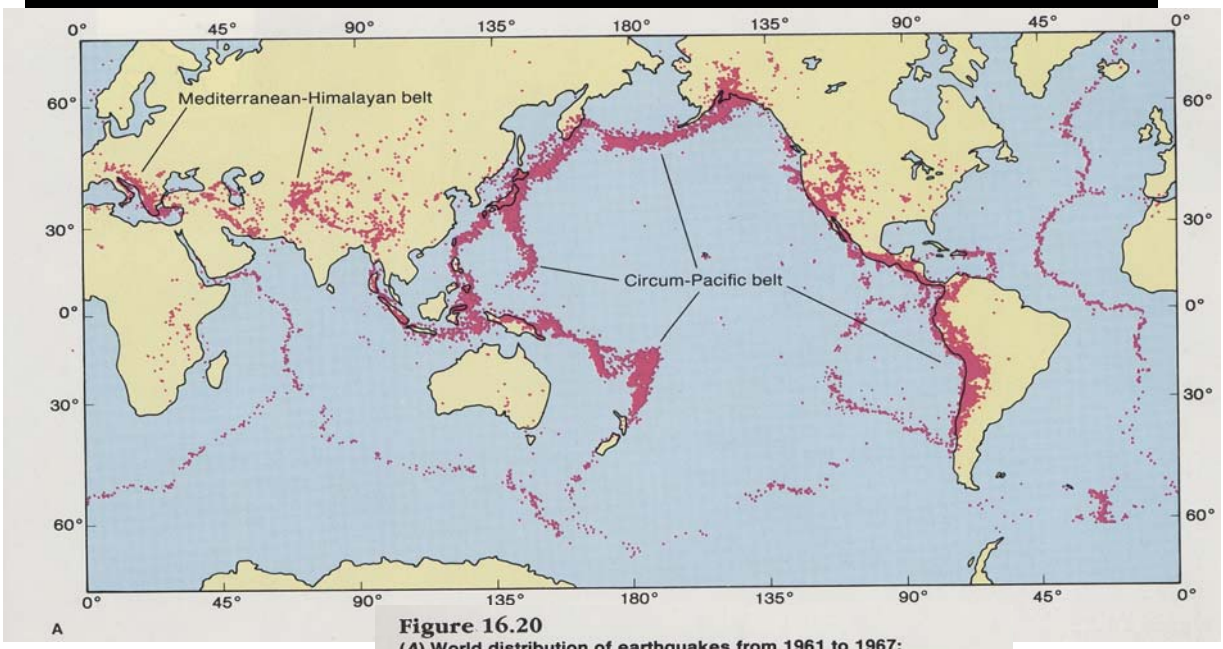
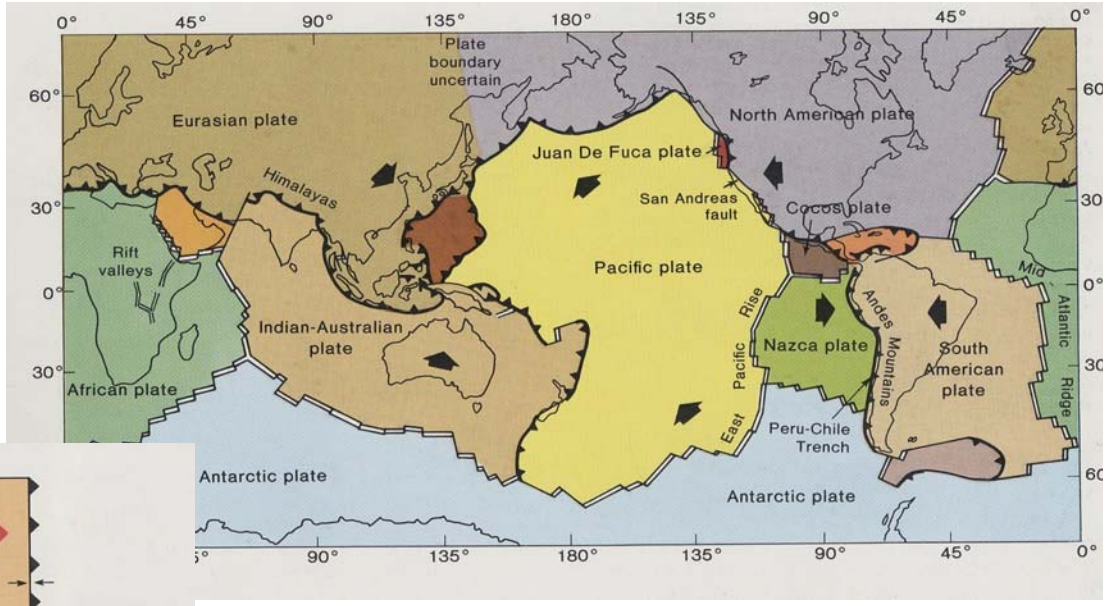


Figure 16.20
(*A*) World distribution of earthquakes from 1961 to 1967; epicenters of quakes with depth of focus between 0 and 700 kilometers. A map of quakes during the 1970s or 1980s would show the same pattern.
From Barazangi and Dorman, *Bulletin of Seismological Society of America*, 1969.



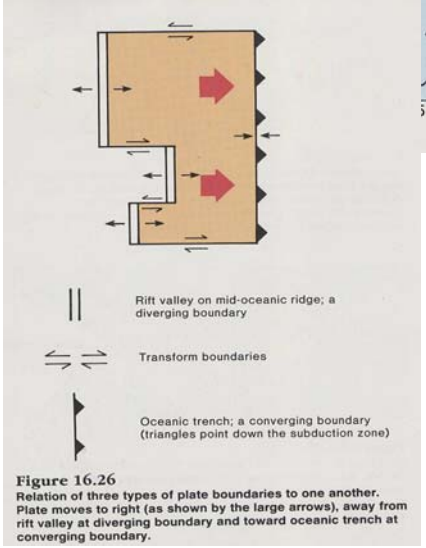


Figure 16.26
Relation of three types of plate boundaries to one another. Plate moves to right (as shown by the large arrows), away from rift valley at diverging boundary and toward oceanic trench at converging boundary.

(*B*) The major plates of the world in the theory of plate tectonics. Compare the locations of plate boundaries with earthquake locations shown in figure 16.20*A*. Double lines show diverging plate boundaries, single lines show transform boundaries. Heavy lines with triangles show converging boundaries; triangles point down subduction zone.
Modified from Hamilton, U.S. Geological Survey.

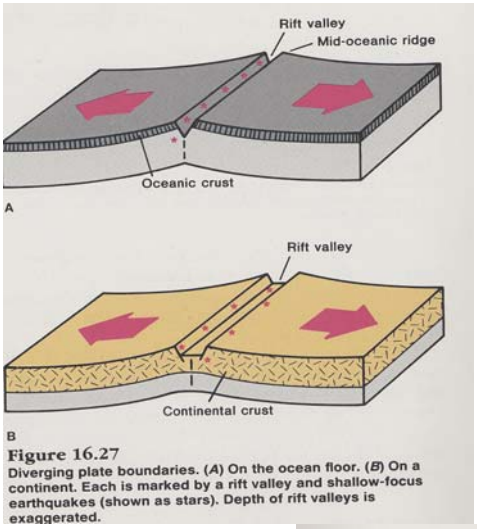


Figure 16.27
Diverging plate boundaries. (*A*) On the ocean floor. (*B*) On a continent. Each is marked by a rift valley and shallow-focus earthquakes (shown as stars). Depth of rift valleys is exaggerated.

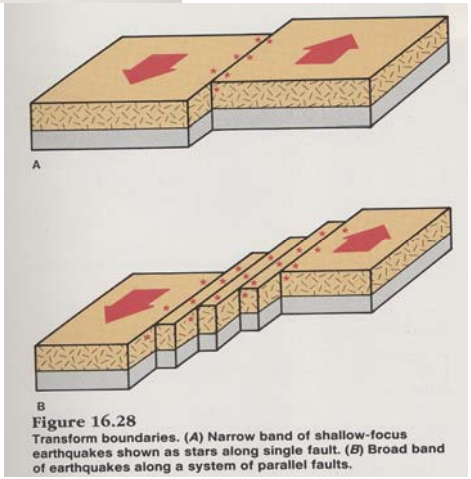


Figure 16.28
Transform boundaries. (*A*) Narrow band of shallow-focus earthquakes shown as stars along single fault. (*B*) Broad band of earthquakes along a system of parallel faults.

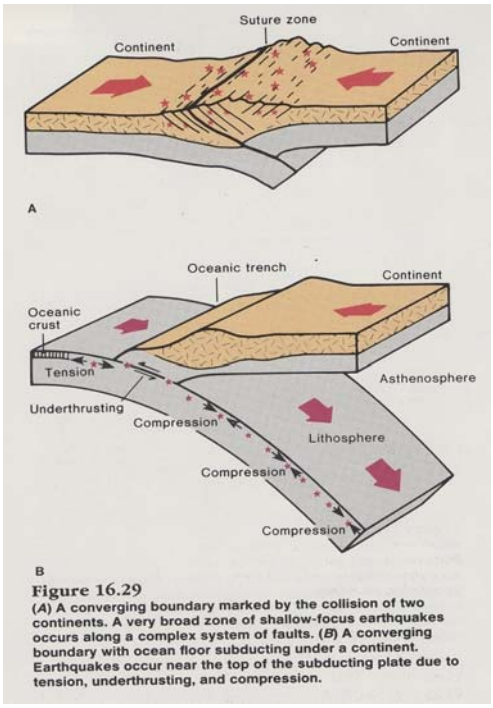


Figure 16.29
(*A*) A converging boundary marked by the collision of two continents. A very broad zone of shallow-focus earthquakes occurs along a complex system of faults. (*B*) A converging boundary with ocean floor subducting under a continent. Earthquakes occur near the top of the subducting plate due to tension, underthrusting, and compression.

8.1.2. Métodos de estudio de fallas activas

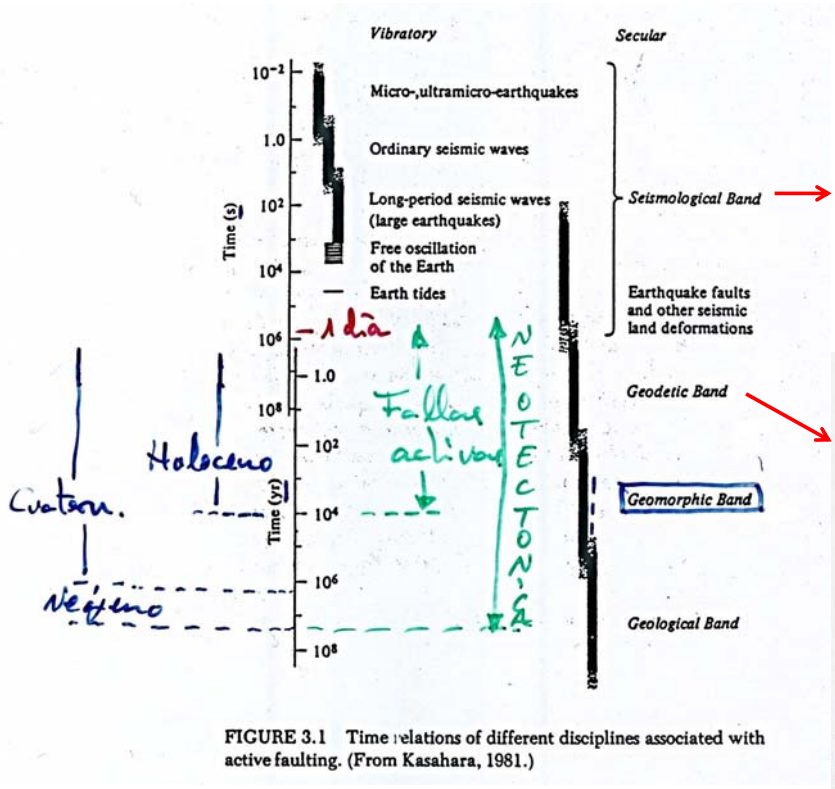
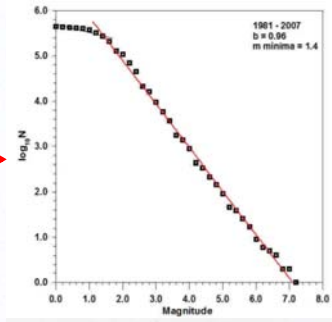


FIGURE 3.1 Time relations of different disciplines associated with active faulting. (From Kasahara, 1981.)



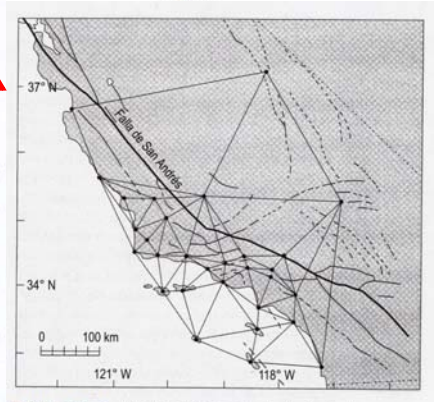


FIGURA 3.12 Red geodésica para el estudio de la deformación, al oeste de la falla de San Andrés, localizada a través de las California Coast Ranges y Continental Borderland. Debido a que el movimiento entre las placas pacífica y norteamericana no se limita a la falla de San Andrés, sino que está distribuida en numerosas fallas, esta densa red se diseñó para determinar exactamente dónde tiene lugar el movimiento (Jordan y Minster, 1988).

8.2. Indicadores geomorfológicos de actividad sismotectónica

8.2.1. Indicadores de fallas normales

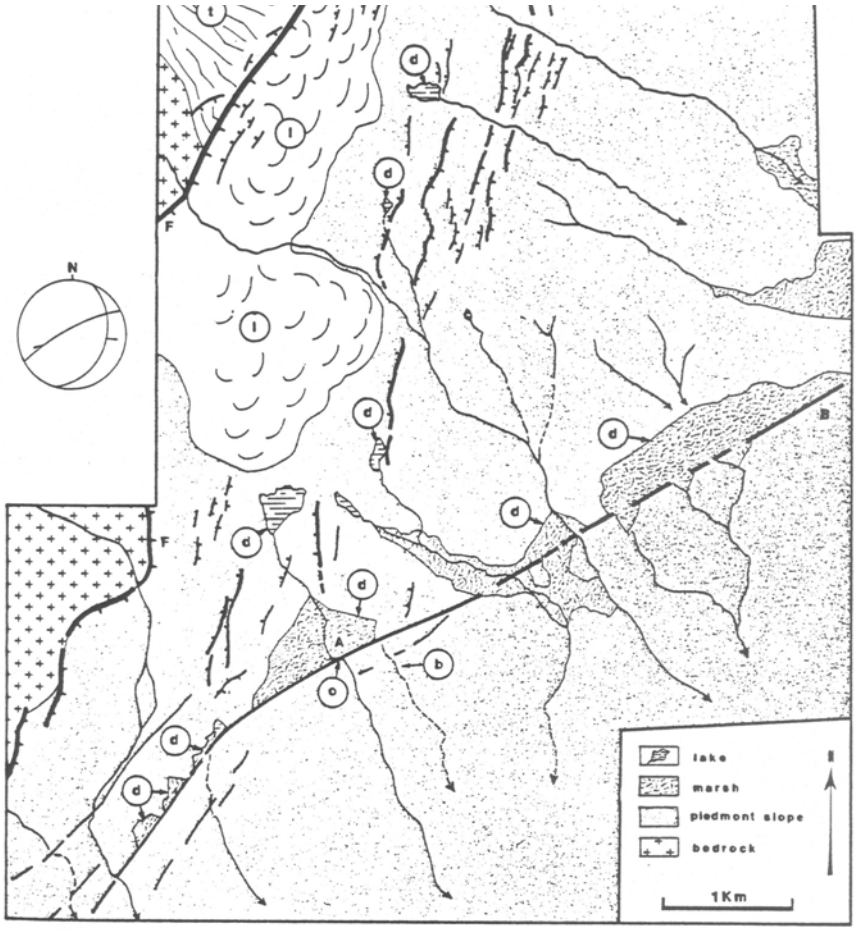
Escarpes de falla







Fig. 23b. Sketch
breaks.



Sketch map corresponding to Figure 14a. F is range front fault. Piedmont slopes are cut by NNE-SSW normal faults and by NW-SW, more linear fault trace (AB), bearing evidence for left-lateral displacement. Attitudes of fault AB and en échelon array are summarized in stereogram (left). Average azimuth of dip-slip scarps within

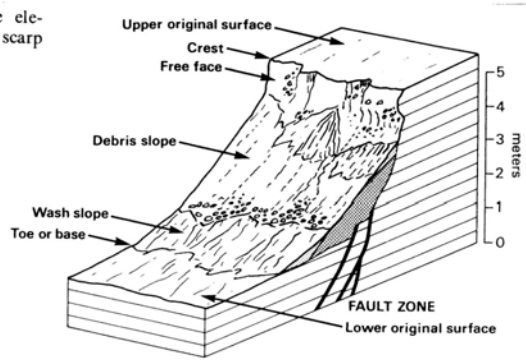
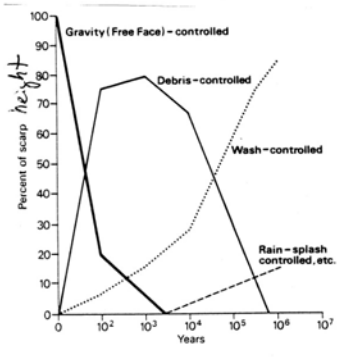


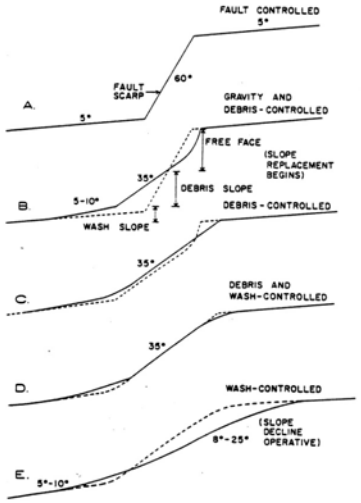
Fig. 6. Generalized slope elements relevant to a fault scarp (after Wallace 1977)

morphology (after Wallace 1977, for fault scarps in the Great Basin,

Slope element	Morphology	Process (formation and/or modification)	Comments and general chronology
Crest	Top of fault scarp (break in slope); initially sharp, becomes rounded with time	Produced by faulting; modified by weathering, mass wasting	Becomes rounded after free face disappears; usually rounded after about 10,000 years
Free face	Straight segment; initially 45° to overhanging	Produced by faulting; modified by weathering, gullying, mass wasting; eventually buried from below by accumulation of debris	Dominant element for 100 years or so; disappears after about 1,000–2,000 years
Debris slope	Straight segment; at angle of repose of material usually 30 to 38°	Accumulation of material that has fallen down from the free face	Is dominant element after about 100 years, remains dominant until about 100,000 years; disappears at about 1,000,000 years
Wash slope	Straight to gently concave segment; overlaps the debris slope; slope angle generally 3 to 15°	Fluvial erosion and deposition; deposition of wedge or fan of alluvium near toe of the slope; some gullying	Is developed by 100 years; significant by 1,000 years; and dominant by 100,000 years
Toe	Base of fault scarp (break in slope) slope; may be initially sharp, but with time may become indeterminate as grades into original slope	Fluvial erosion and deposition; owes to change in process/form from upslope element (free face, debris slope, or wash slope) to original surface below the fault scarp slope	More prominent in young fault scarps or where wash slope is not present. On scarps older than about 12,000 years the basal slope break is sharper than the crestal slope break

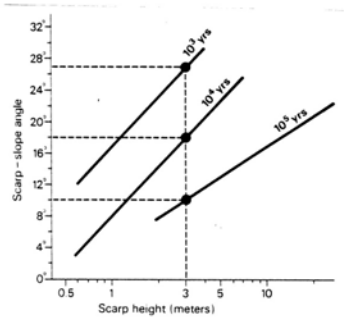


Change in slope elements (fault-scarp morphology) with time for fault-scarp degradation in the Great Basin area of Nevada. After Wallace (1977).

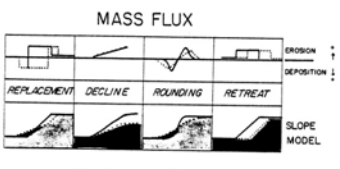


Sequence of fault-scarp degradation. To show incremental change, dotted line represents solid line of previous profile.

Evolución de los procesos y la variación que estos producen en las pendientes durante la degradación de un escarpe.Según Wallace 1977.



Relationship between fault-scarp height and scarp-slope angle from scarps ranging in age from 10^3 and 10^5 yr. After Bucknam and Anderson (1979).



Mass-flux diagram illustrating the differences in slope models in terms of how erosion or deposition is distributed along the profile. The solid lines mark the initial condition, and the dotted lines indicate profile change after some time. On the lower portion of the figure, white areas of the profile indicate erosion while the dark areas (for rounding and replacement) indicate deposition.

8.2.2. Indicadores de fallas inversas y cabalgamientos

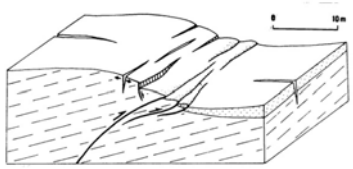


Fig. 13. Diagram showing the different break types in the zone A.

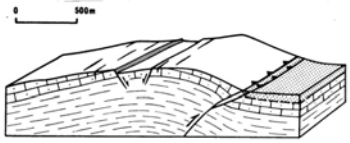


Fig. 15. Diagram showing the structure of the zone B.

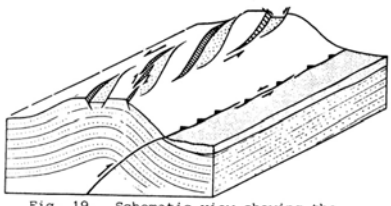


Fig. 19. Schematic view showing the structures of the zone C.



Fig. 14. Map of a graben on a fold extrados. 1, Normal faults. 2, Tensile crac 3, Pressures ridges and thrust faults. 4, Dip angle of the bedding plane.

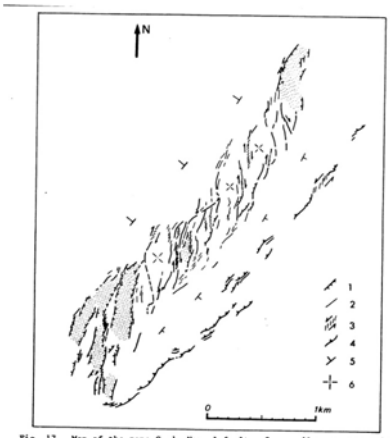


Fig. 17. Map of the zone C. 1, Normal faults. 2, tensile cracks, 3, 'en échelon' cracks. 4, thrust faults and pressure ridges. 5, dip angle of th bedding plane. 6, horizontal stratification.

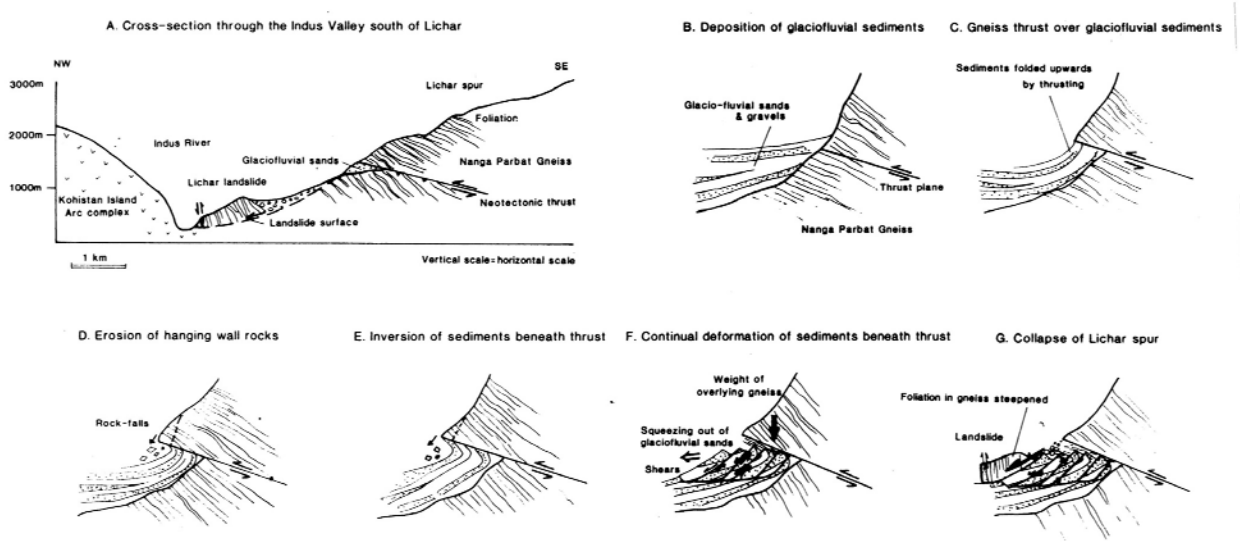
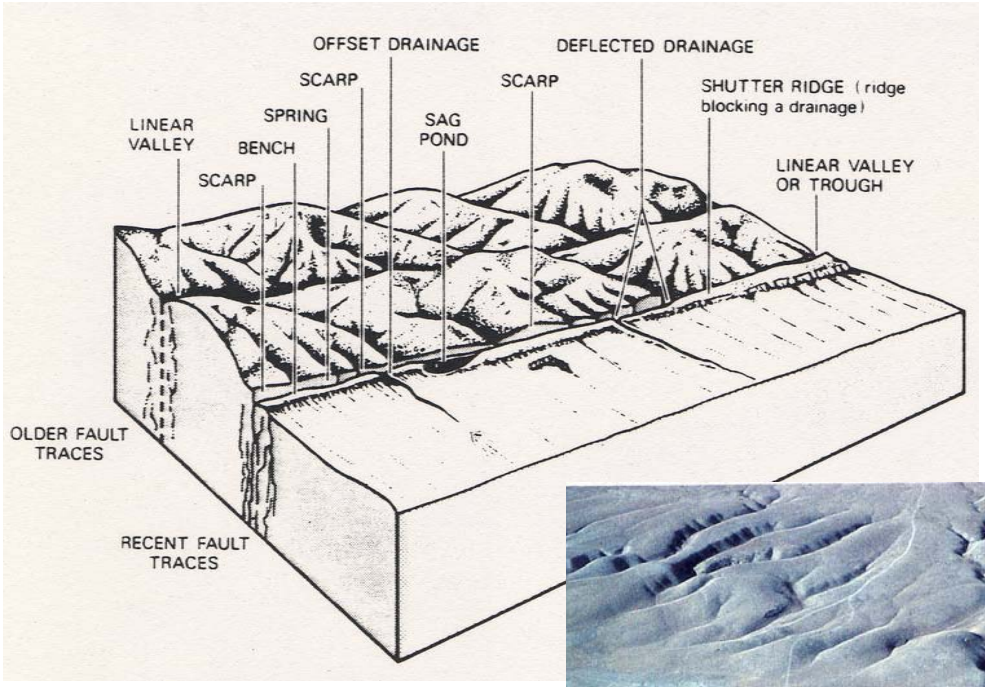


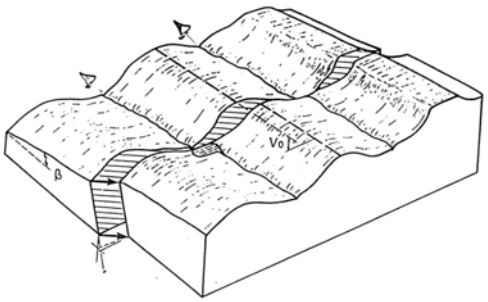
Fig. 12. A. Cross-section across the Indus valley south of Lichar village. B–G. A model for the development of the area around the Lichar spur.

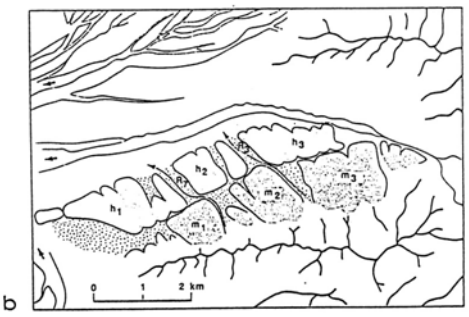
8.2.3. Indicadores de fallas de desgarre





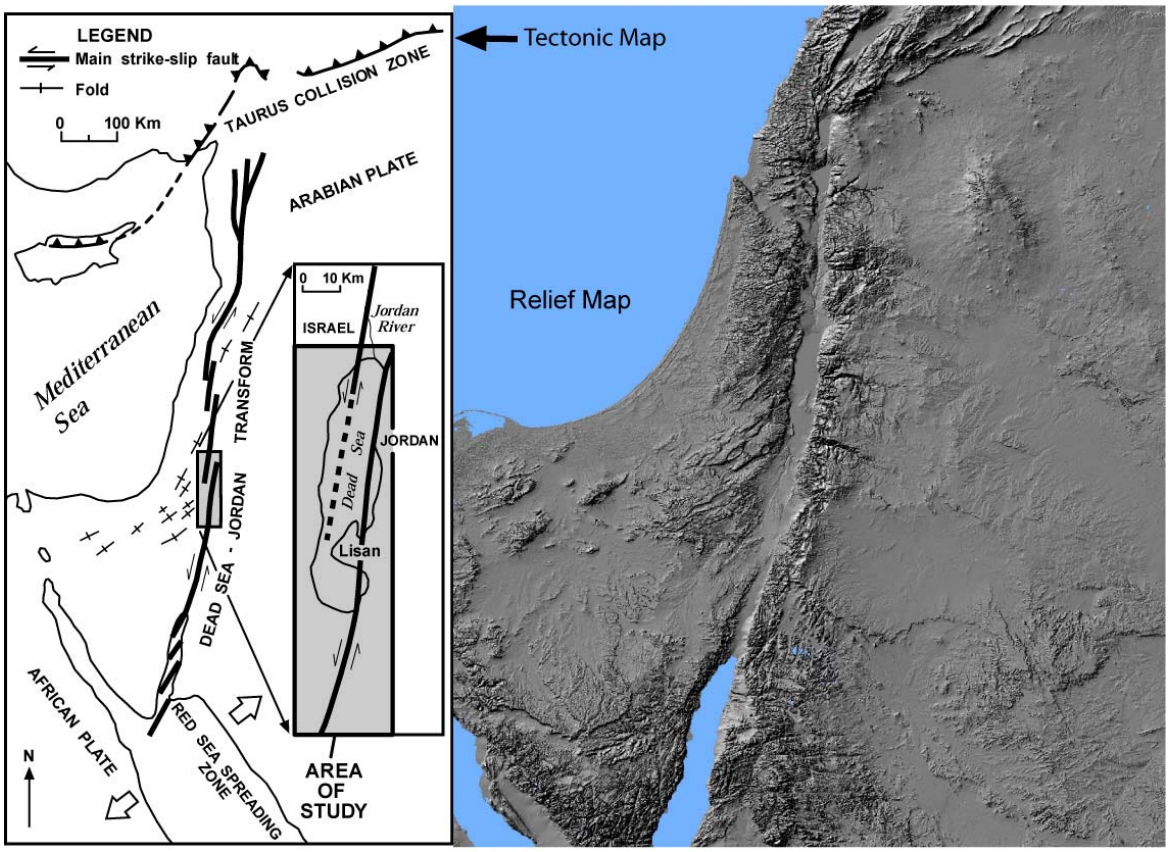








Tectonic elements (left) and shaded relief of the topography (right) of the Dead Sea Transform.





Falla de San Andrés

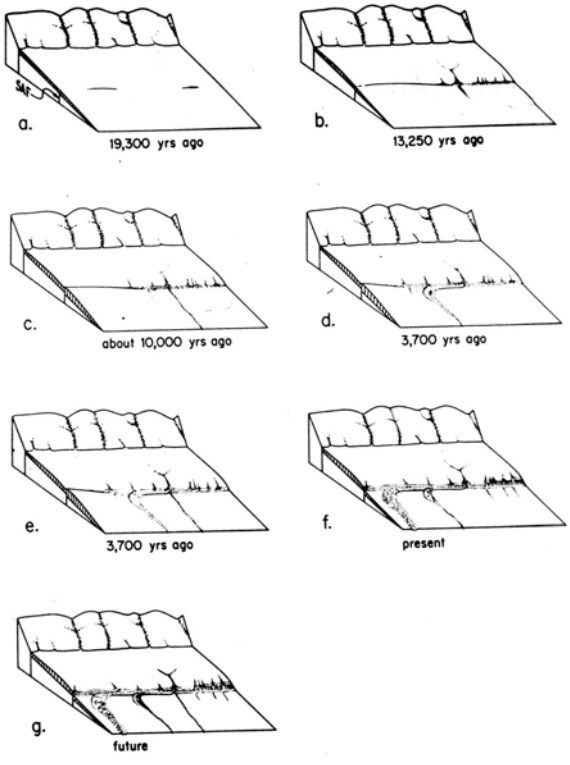
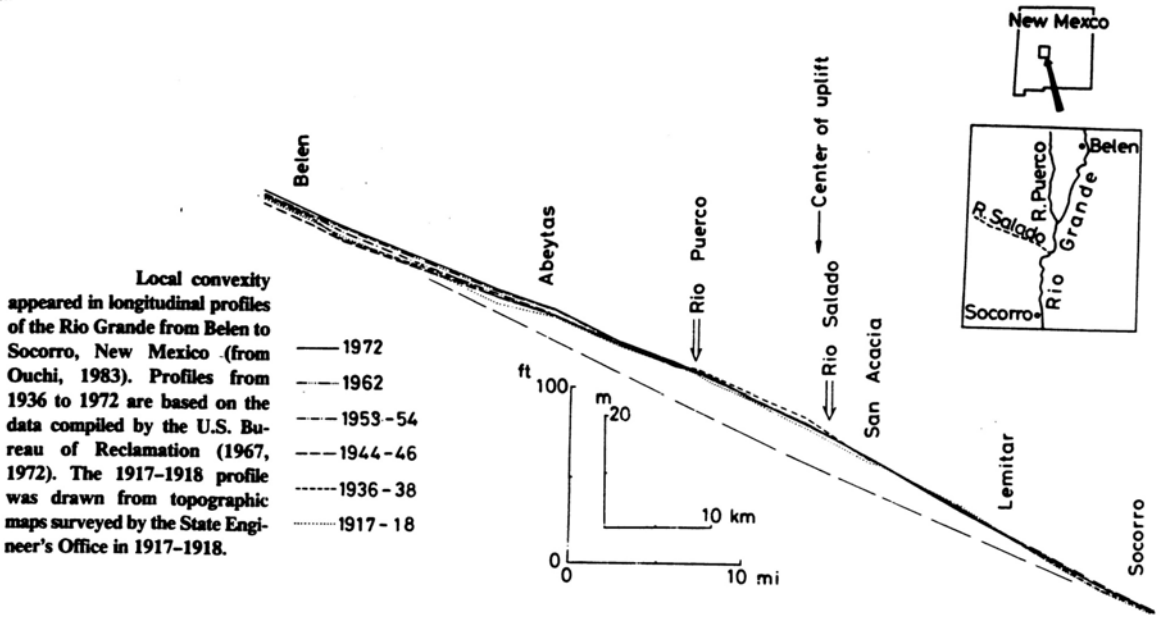


Figure 7. The Holocene–late Pleistocene evolution of Wallace Creek. An aggrading "older alluvial fan" during the period including 19,300 yr ago progressively buried small scarps formed along the San Andreas fault (SAF) during major strike-slip events (a). Right-lateral offsets accumulated during this period, but no geomorphologically recognizable offsets began to form until 13,250 yr ago, when the "older alluvial fan" became inactivated by initial entrenchment of Wallace Creek (b). At this time, erosion of small gullies to the right (southeast) of Wallace Creek also resulted in deposition of the "younger fan alluvium" downstream from the fault. These features then began to record right-lateral offset, and scarps began to grow along the fault. About 10,000 yr ago, a new channel was cut across the fault at Wallace Creek, and the initial channel, downstream from the fault, was abandoned (c). The new channel remained the active channel of Wallace Creek during the early and middle Holocene, during which ~250 m of slip accumulated (d). This channel filled with "high-channel alluvium" 3,700 yr ago, and Wallace Creek cut a new channel straight across the fault (e). Between 3,700 yr ago and the present, this youngest channel has registered 128 m of right-lateral offset (f). Aggradation of this channel, accompanied by continued offset, will probably lead to its abandonment and the creation of a new channel, cut straight across the fault (g).

8.2.3. Indicadores de pliegues



Local convexity appeared in longitudinal profiles of the Rio Grande from Belen to Socorro, New Mexico (from Ouchi, 1983). Profiles from 1936 to 1972 are based on the data compiled by the U.S. Bureau of Reclamation (1967, 1972). The 1917–1918 profile was drawn from topographic maps surveyed by the State Engineer's Office in 1917–1918.

Fig 19.- Perfiles longitudinales a lo largo del Río Grande según bases topográficas diferentes. Todas ellas muestran una convexidad en el centro. Según Ouchi 1985.

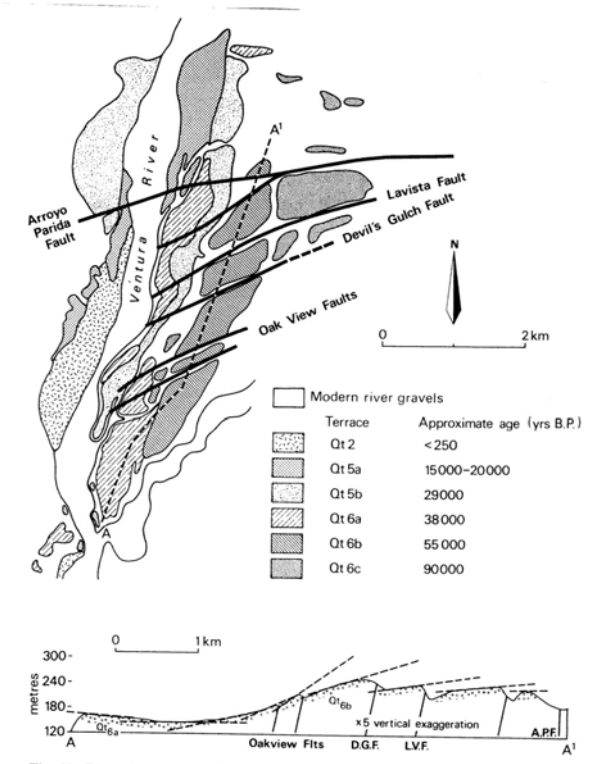
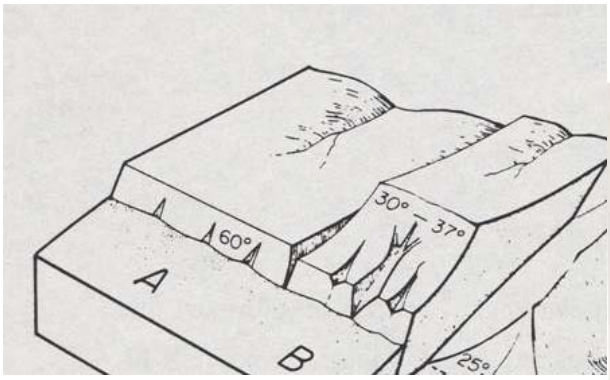
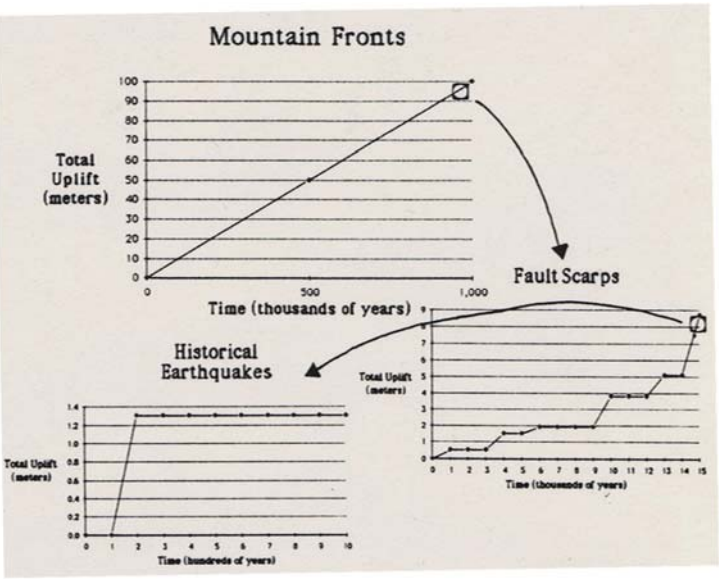


Fig. 13. Fluvial terraces of the Venture River, California, deformed by folding and faulting. (after Keller et al. 1982 b)

8.3. Indicadores del grado y duración de la actividad

Frentes montañosos









Facetas triangulares en frentes montañosos

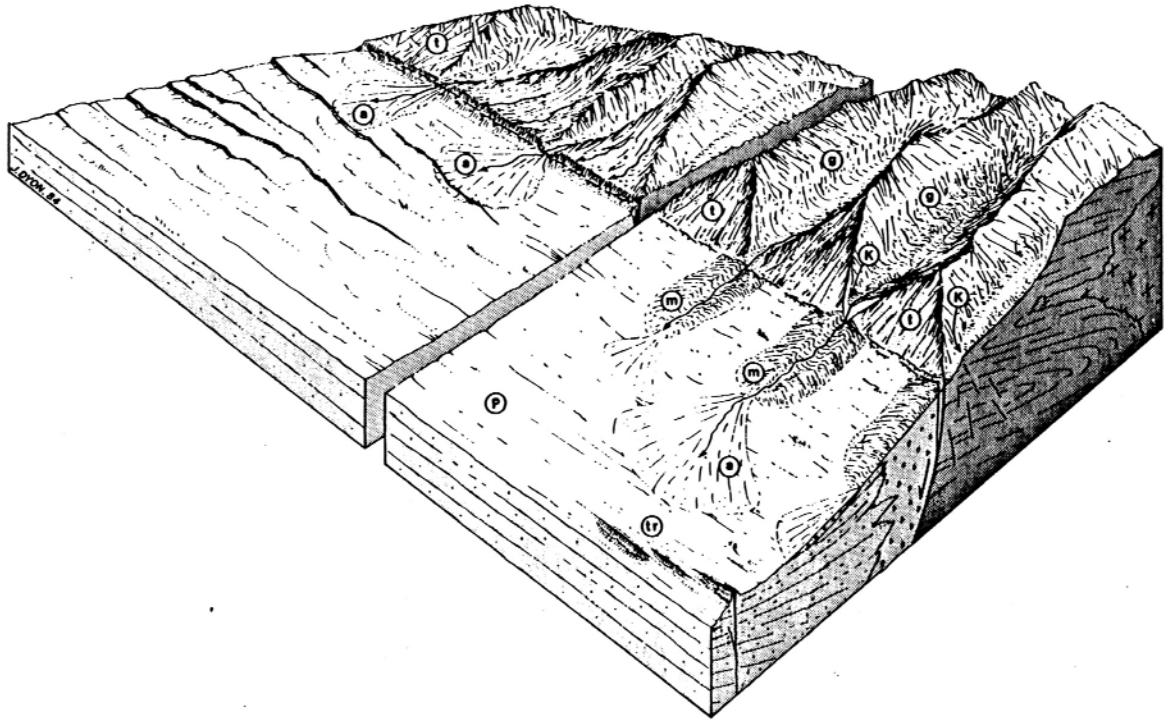


Fig. 1. Summary of typical morphological features along normal faults in Tibet. Left side represents faulted graben floor (e.g., Figure 10) and mountain front with steep young scarp but degraded triangular facets (t) (e.g., Figure 24). Right side represents mountain front with steeper facets (t) and perched glacial valleys (g) (e.g., Figure 3). m, moraines; k, knick; a,p, alluvial fan, plain; tr, travertine ridge.





Valles en botella

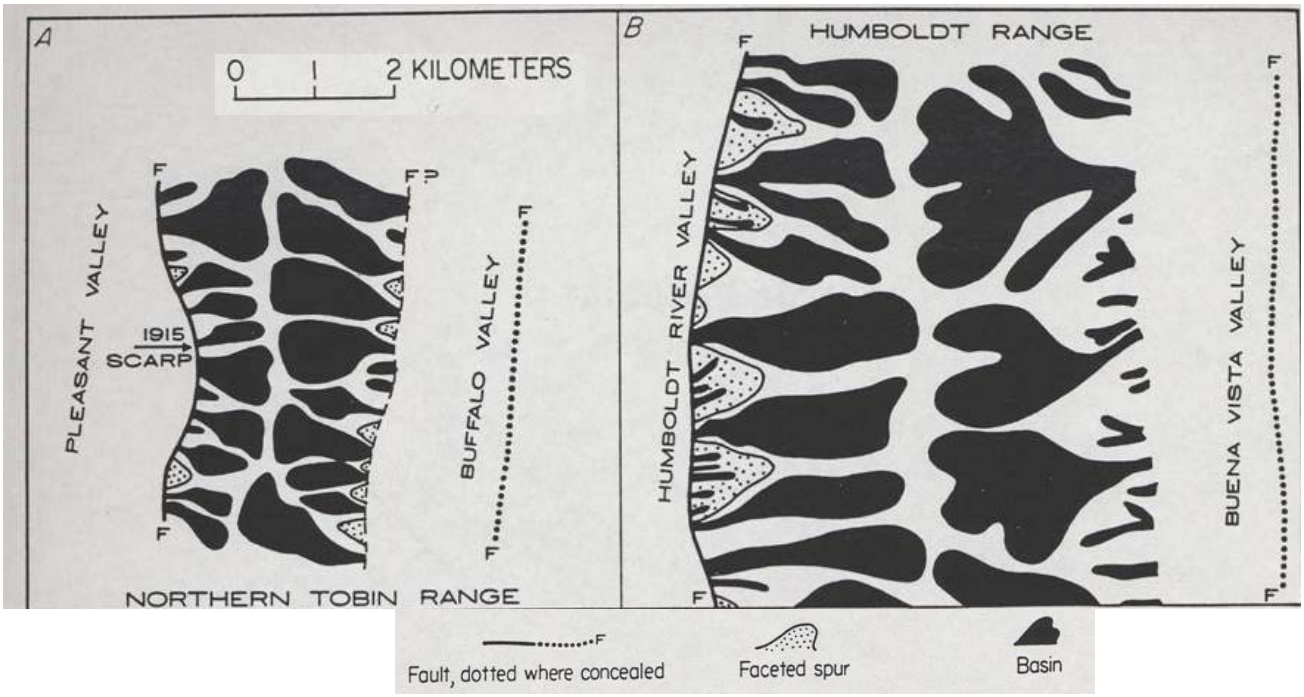
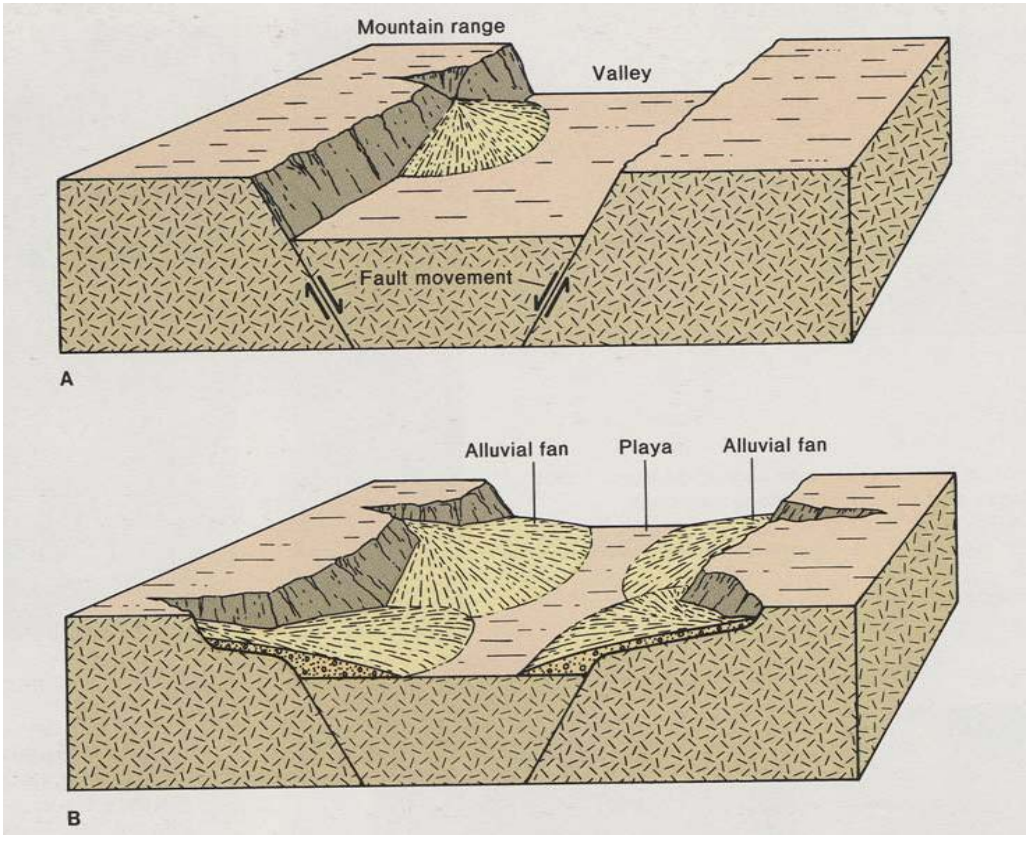
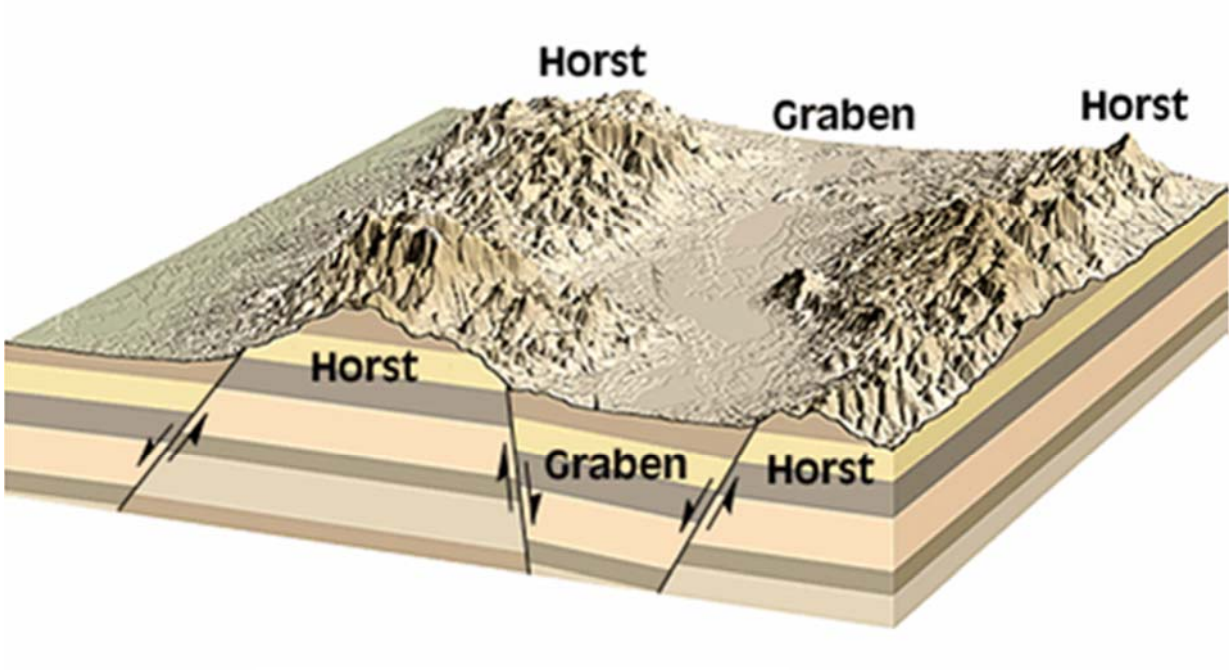


Fig. 2.7. Exemples de la disposició de les conques de drenatge en fronts muntanyosos generats per falles neotectòniques. En general s'estrenyen just en l'arribar al front donant lloc a les formes *wine glass*. Aquestes formes s'observen a la figura en les dues vessants del *Northern Tobin Range*, i en la vessant de *Humboldt River Valley* a *Humboldt Range* en les seves formes més característiques (De Wallace 1978).

Fosas tectónicas y su relleno sedimentario



Sierras y depresiones tectónicas



Graben = fosa tectónica

Evolución de un frente montañoso

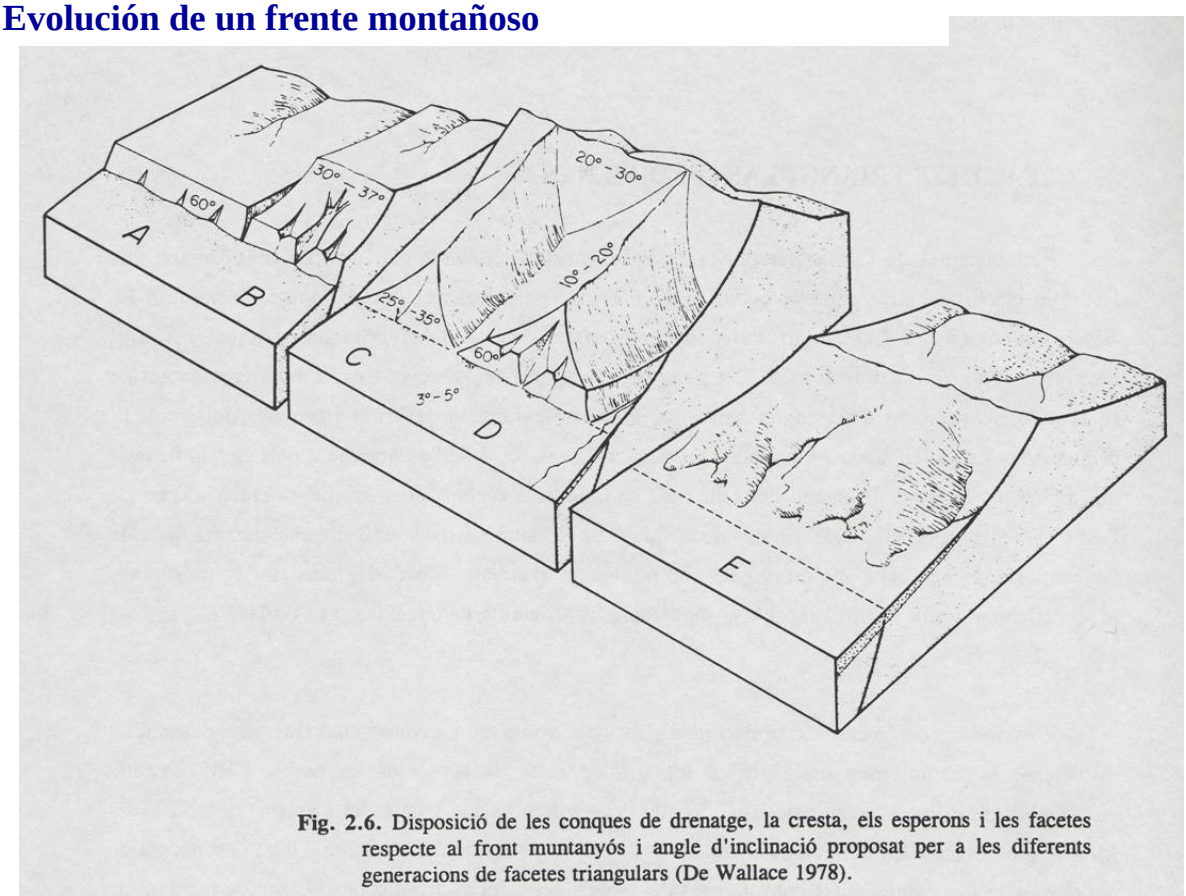
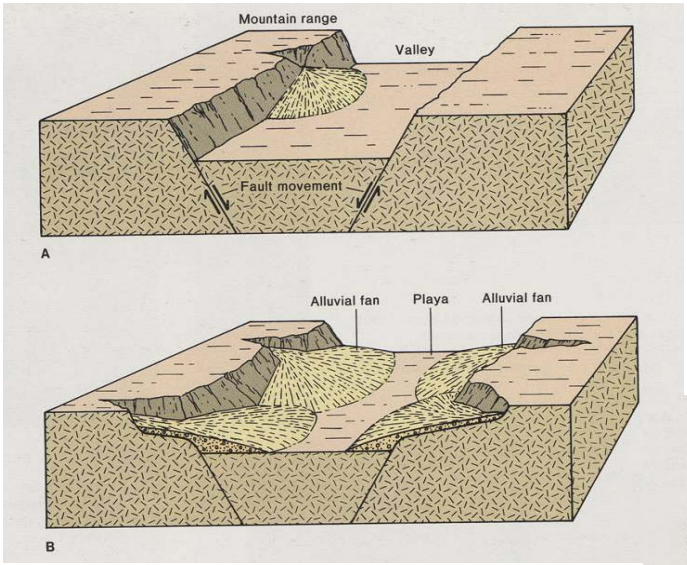
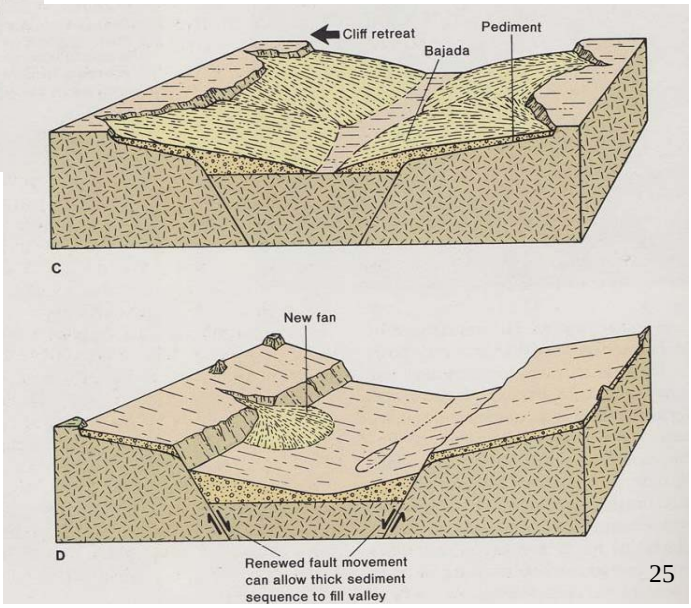


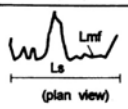
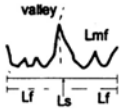
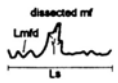
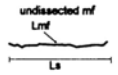
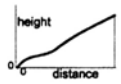
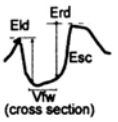
Fig. 2.6. Disposició de les conques de drenatge, la cresta, els esperons i les facetes respecte al front muntanyós i angle d'inclinació proposat per a les diferents generacions de facetes triangulars (De Wallace 1978).





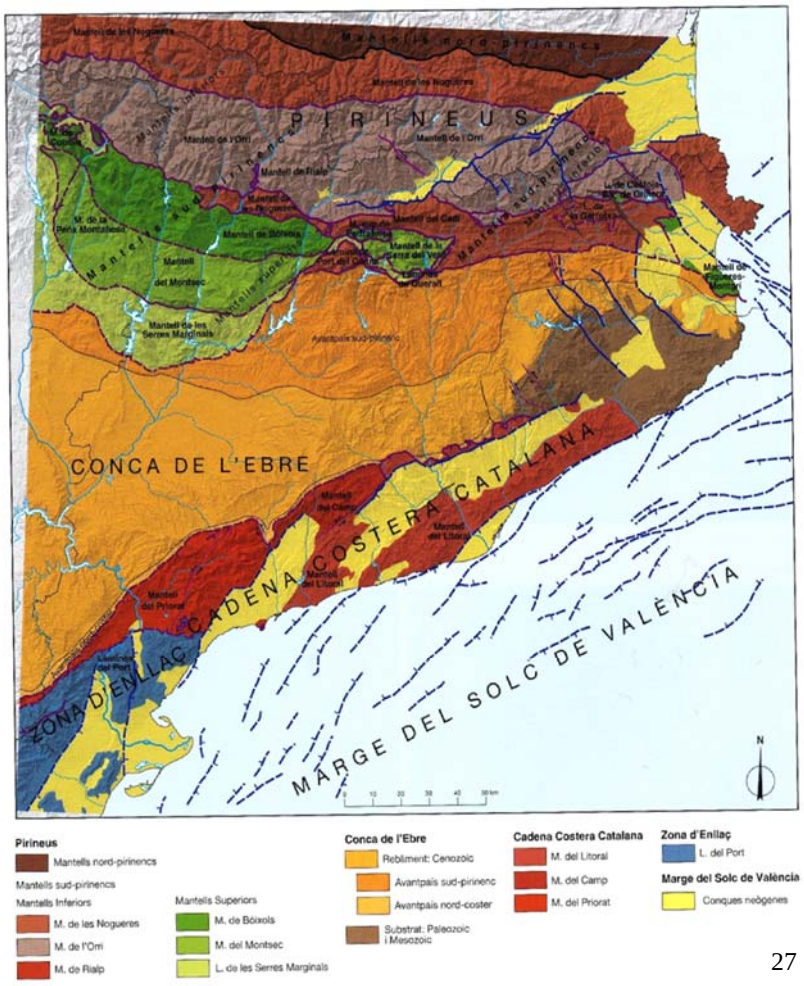
Determinación del grado de actividad

Table I. Summary of the morphometric parameters used in tectonic landform analysis of individual mountain fronts of the Acambay graben (after Wells *et al.*, 1988)

Morphometric parameter	Mathematical derivation*	Measurement Procedure	Purpose	Significance	Source
S_{mf} - Mountain front sinuosity	$S_{mf}=L_{mf}/L_s$		Reflect a balance between the tendency of stream and slope processes to produce irregular (sinuous) mountain front and vertical active tectonics that tend to produce a prominent straight front (Keller, 1986)	S_{mf}= 1·0 – most tectonic activity S_{mf}> 1·0 – less tectonic activity	Bull and McFadden, 1977
Percentage faceting along mountain fronts	L_f/L_s		Define the proportion of a mountain front that has well defined triangular facets, using the ratio of the cumulative lengths of facets to overall mountain front length	Tectonically active fronts display prominent, large facets that are generated and/or maintained by recurrent faulting along the base of the escarpments, i.e. high percentage faceting	Wells *et al.*, 1988
F_d, Percentage dissected mountain fronts	L_{mfd}/L_s		Define the proportion of a mountain front that has been dissected into distinct facets	Most tectonically active mountain fronts tend to be less dissected, i.e. low F_d values	Wells *et al.*, 1988
E_u, Percentage undissected escarpments	L_{ce}/L_s		Define the proportion of a mountain front that has not been dissected	Most tectonically active mountain fronts show laterally continuous undissected escarpments, i.e. high E_u values	This study
Stream long-profiles			Define any irregularities in channel slope that reflect disequilibrium conditions	Disequilibrium conditions suggest tectonic disruption of the bed	Hack, 1973
V_f, Valley floor – valley height ratio	$V_f=2V_{fw}/[(E_{ld}-E_{sc})+(E_{rd}-E_{sc})]$		Define the ratio of the width of the valley floor to the mean height of two adjacent divides	The index reflects differences between broad-floored canyons with relatively high values of V_f, and V-shaped canyons with relatively low V_f values	Bull and McFadden, 1977
B_s, Drainage basin shape ratio	$B_s=B_l/B_w$		Define the planimetric shape of a basin	High B_s values = elongated basins, i.e. high tectonic activity; low B_s values = circular basins, i.e. low tectonic activity	This study, after Cannon (1976)

* symbols: L_{mf}—length of mountain front along the mountain-piedmont junction, L_s—straight-line length of the front, L_f—cumulative lengths of facets, L_{mfd}—the length of dissected mountain front, L_{ce}—cumulative length of all laterally continuous undissected escarpments, V_{fw}—width of valley floor, E_{ld} and E_{rd}—respective elevations of the left and right valley divides and E_{sc}—elevation of the valley floor, B_l—length of the basin, measured from its mouth to the most distant drainage divide, B_w—width of the basin measured across the short axis.

Ejemplo de fosa tectónica: fosas neógenas de la Cordillera Costera Catalana



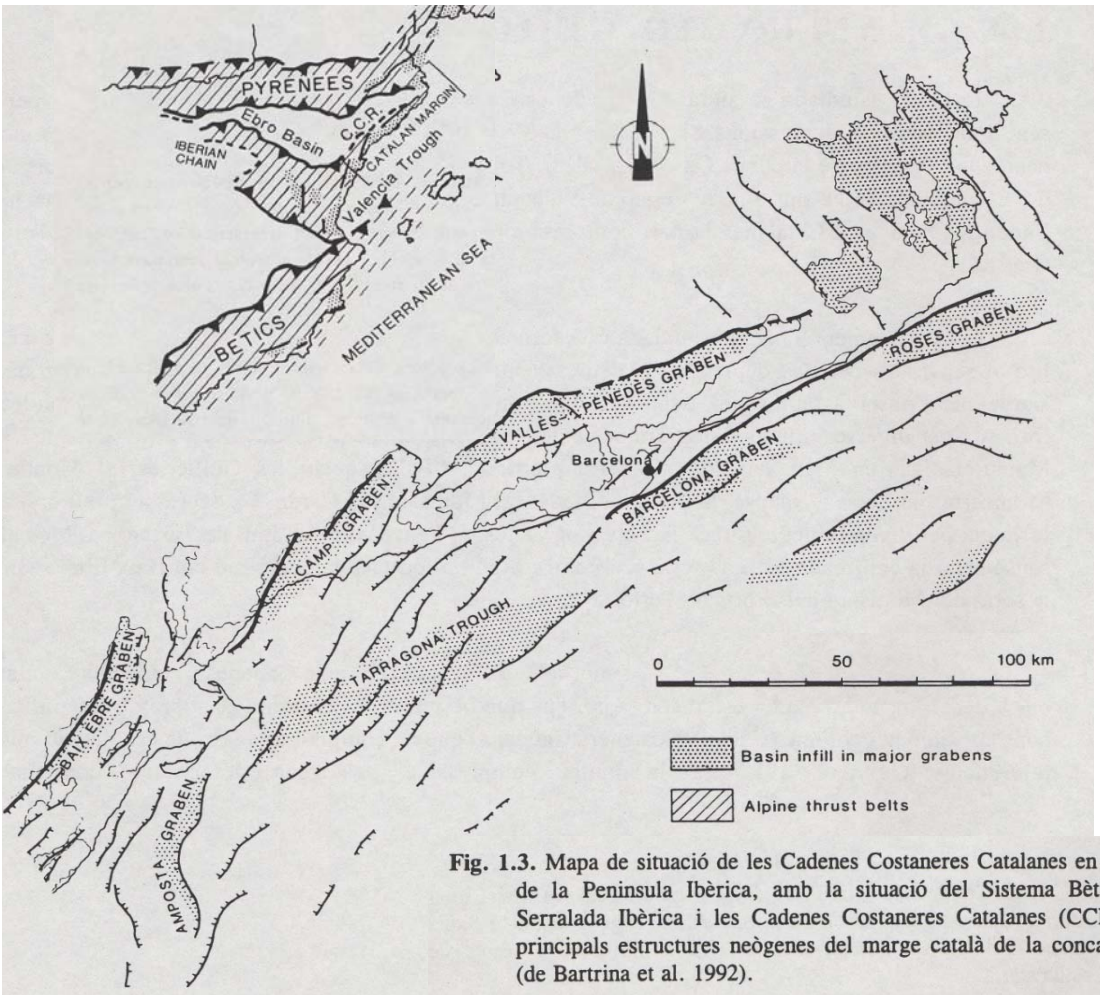
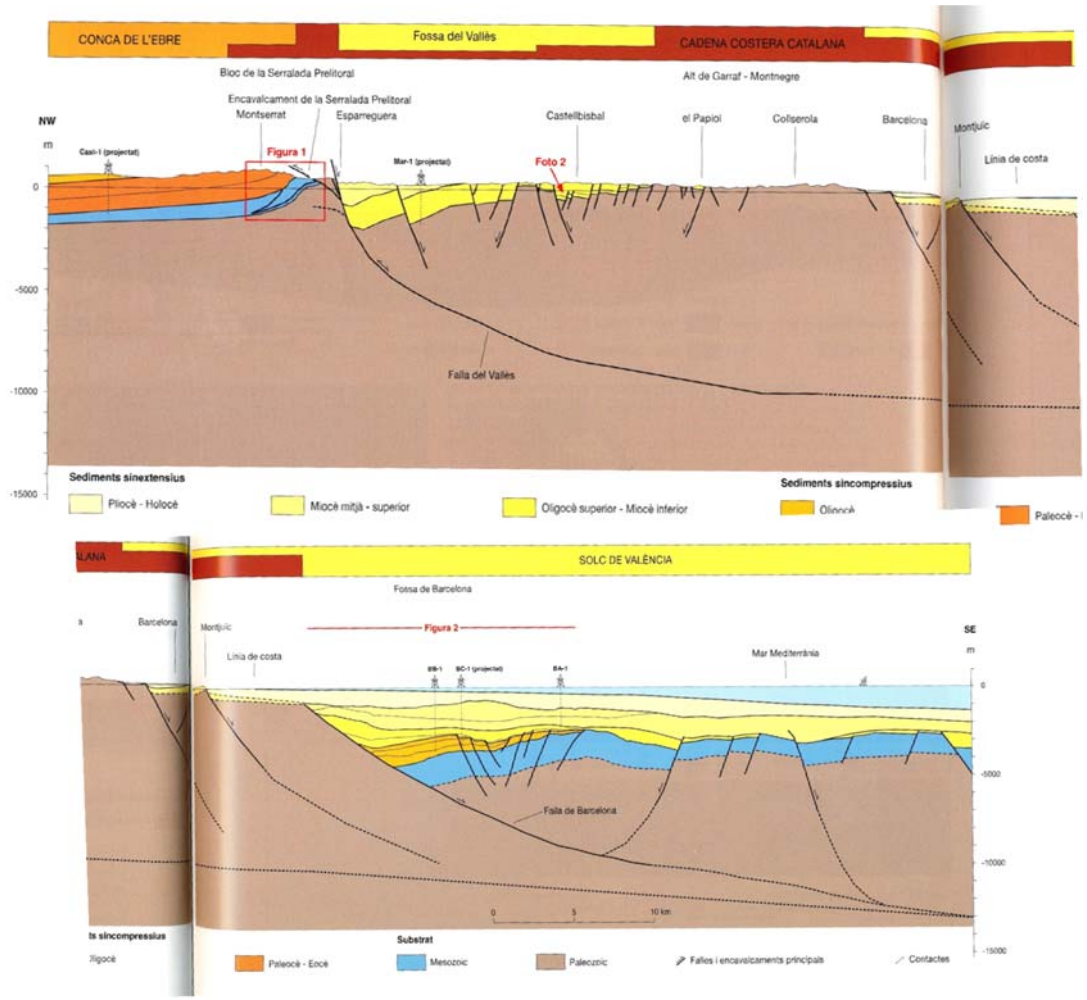
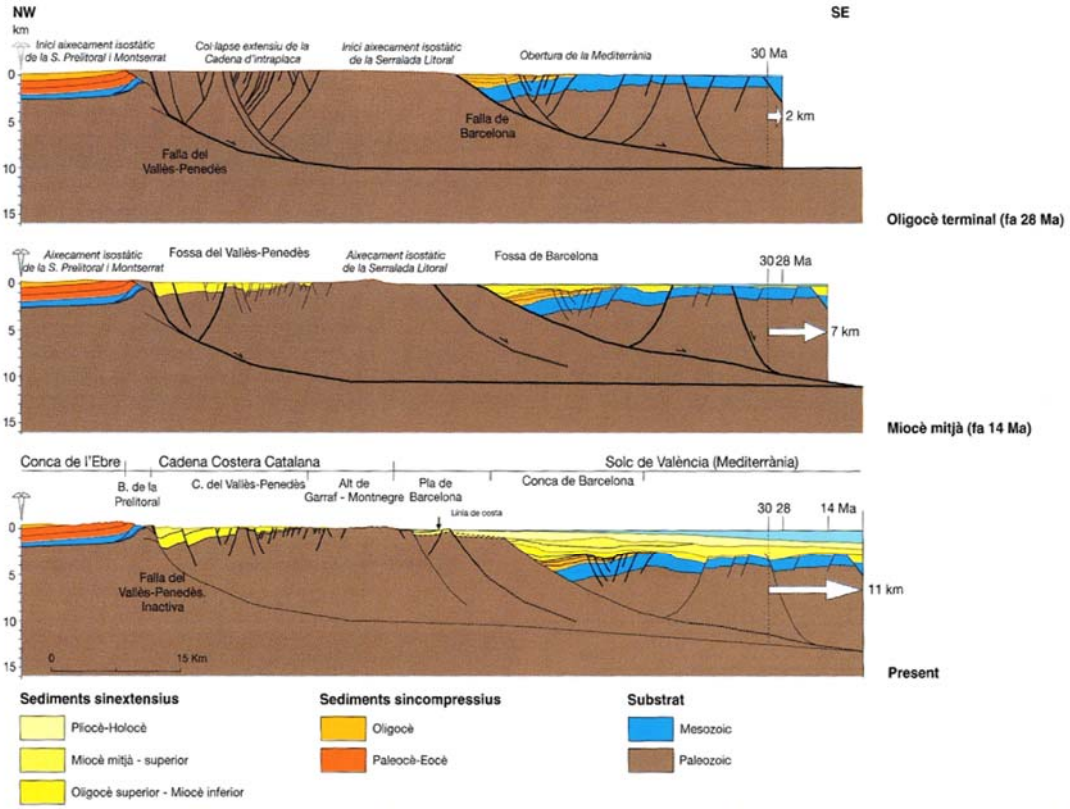


Fig. 1.3. Mapa de situació de les Cadenes Costaneres Catalanes en el context del NE de la Peninsula Ibèrica, amb la situació del Sistema Bètic, el Pirineu, la Serralada Ibèrica i les Cadenes Costaneres Catalanes (CCR) i mapa de les principals estructures neògenes del marge català de la conca Catalano-Balear. (de Bartrina et al. 1992).



29

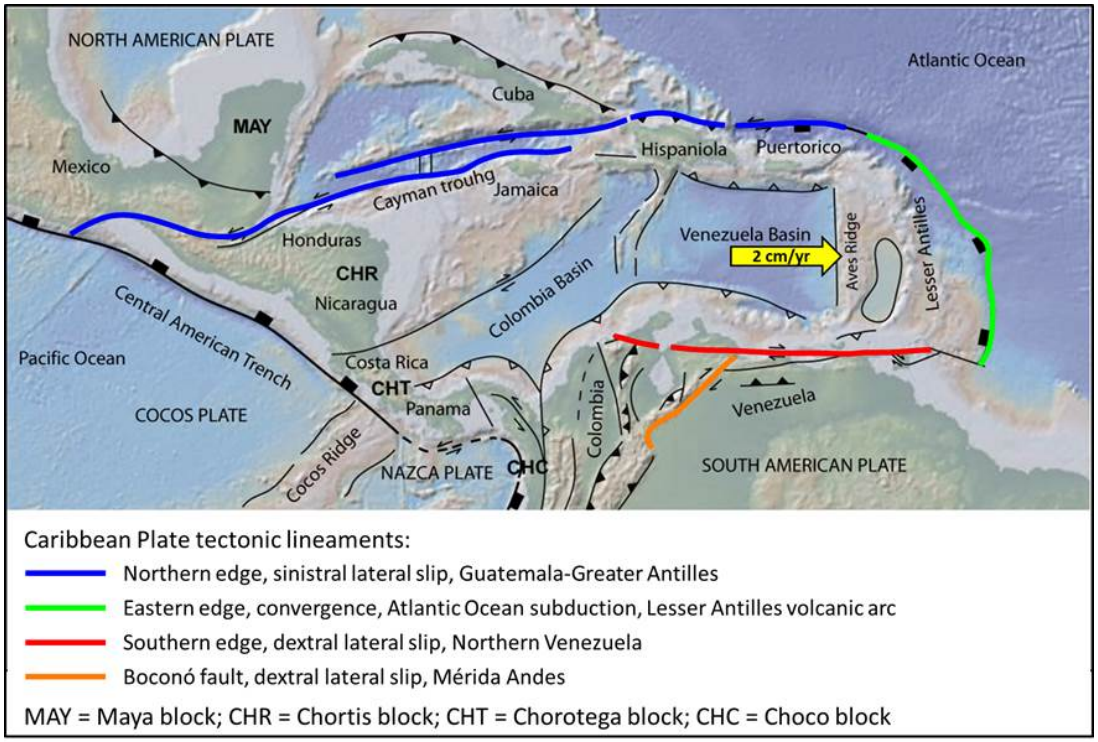
Etapa extensiva (28 a 0 Ma): la formació de les conques i l'obertura de la Mediterrània



3: Seqüència de talls restituïts representatius de l'evolució de la Cadena Costera Catalana des de l'Eocè fins avui; s'hi indiquen l'escurçament i l'estirament acumulats per a cada estadi.

30

8.4. Neotectónica de la placa del Caribe



Caribbean Plate tectonic lineaments:

- Northern edge, sinistral lateral slip, Guatemala-Greater Antilles
- Eastern edge, convergence, Atlantic Ocean subduction, Lesser Antilles volcanic arc
- Southern edge, dextral lateral slip, Northern Venezuela
- Boconó fault, dextral lateral slip, Mérida Andes

MAY = Maya block; CHR = Chortis block; CHT = Chorotega block; CHC = Choco block

